Astron. Astrophys. 213, 502–515 (1989)

ASTRONOMY AND ASTROPHYSICS

The implications of image scrambling and focal ratio degradation in fibre optics on the design of astronomical instrumentation

C.A. Clayton *

Department of Astronomy, University of Manchester, Manchester M13 9PL, United Kingdom

Received August 1, accepted August 26, 1988

Summary. A review of Image Scrambling (IS) and Focal Ratio Degradation (FRD) in both straight and bent fibre optic cables is presented. This work has been undertaken in an attempt to determine how these phenomena will affect the performance of astronomical instrumentation incorporating fibre optics, with reference in particular to the Manchester echelle spectrometers. The results from an experimental investigation into these phenomena then follows. This investigation includes a comparison of the relative amounts of FRD due to diffraction, microbends and macrobends; a comparison of FRD performance of different "astronomical" fibres as a function of bend radius; an examination of the effects of localised stress on FRD and severe bending in short fibres, and finally the IS properties of short fibres.

The most important conclusions drawn from these experiments are that: 1) Localised stress dominates FRD. 2) Macrobends on the scale normally encountered in current instruments are shown not to contribute significantly to FRD. 3) IS is incomplete in short (few cm) fibres. 4) The position of a source on a fibre dictates the transmission efficiency.

Key words: instruments – spectroscopy

1. Introduction

The use of total internal reflection as a means of conveying light was well known to the designers of illuminated fountains in the 19th century and was the subject of an occasional scientific demonstration (Tyndall, 1854). The application of this phenomenon to small fibres was suggested in the early 1900s. A practical form of fibre optics, however, did not emerge until the concept of a transparent optical coating was proposed by Heel (1954). The use of such a "cladding" layer provides a protected interface for total internal reflection and prevents leakage of light between adjacent fibres. In the absence of such a coating, most fibres are so inefficient that they are of little practical use. This was a major breakthrough and since then fibre optics have found many uses in applications as diverse as surgical instrumentation, military cyphers and even astronomy.

The first recorded suggestion of using fibre optics in an astronomical application was made by Kapany (1955) at a symposium on astronomical optics held at Manchester University. He suggested using an assembly of fibres to transform the shape of a beam of light. In particular, with stellar spectrographs, a circular bundle of fibres can be placed at the star image, and the other ends of the fibres made to lie in a row, forming the slit of the spectrograph. This greatly increases the amount of light from the star reaching the instrument with would otherwise have been lost due to seeing effects and tracking errors.

This technique of image reformatting is precisely that aspect of fibre optics which is to be discussed in this paper, with respect to use with the Manchester echelle spectrometers (Meaburn et al., 1984). In this case, we are not attempting to combat the effects of seeing but are trying to optimise the use of the long slit of the echelles when observing objects which do not extend along the entire length of the slit. Such objects include extragalactic H II regions, galactic nuclei and planetary nebulae. By suitable image reformatting, the entire object can be observing in a single integration as opposed to systematically stepping the slit across the target. Clearly this represents a very efficient use of telescope time.

Alternatively, we might use image reformatters on extended objects to sample emission from, say, a grid of widely spaced points. Such an array may be used on galactic H II regions to search for regions of high velocity motion or, in the secondary low dispersion mode of the echelles, to measure variations in abundance over a large area of an object. A more closely spaced array could also be used to emulate the imaging Fabry-Perot interferometer, Taurus (Taylor and Atherton, 1980).

The use of fibres instead of conventional optics in astronomical instrumentation has occurred, despite the major drawback of their lower transmission efficiency, because of several important properties of fibres (Lund, 1984).

Firstly, the small size of fibres means they can be introduced into small confined spaces. In applications where independent light sources need to be combined in a closely packed arrangement (such as in multi-object spectroscopy) fibres can provide a convenient solution.

Secondly, the flexibility of fibres has many mechanical advantages in astronomical instrumentation such as the possibility of isolating instruments from the telescope, thereby eliminating the need for heavy and rigid structures which must be intermittently attached to and removed from the telescope. Some instrument changes could be achieved in minutes.

Thirdly, the important property of image scrambling (IS) occurs in certain types of fibres. Multiple reflections occurring

* Present address: Institute of Astronomy, Madingley Road, Cambridge CB3 OHA, United Kingdom

within a long fibre tend to integrate any variations in illumination across its entrance aperture (due to, say, seeing) so that the exit aperture of the fibre appears uniformly bright. This can be very useful in applications where the symmetrical and time-independent illumination of an instrument is desired as, for example, in high resolution spectrographic radial velocity determinations.

Lastly, and by no means least, a fibre linked instrument can prove considerably cheaper than the alternative solution involving classical optical components. In addition, the high efficiency of multi-object fibre spectroscopy can provide huge saving in terms of telescope time. It is towards this last application that most attention has been paid to date by astronomers around the world.

The first working multiple-fibre spectrograph was built and used by Hill et al. (1980, 1982). Their system, MEDUSA, links the Cassegrain focal plane of the Steward 2.3 m telescope to a spectrograph (mounted immediately behind) with up to 40 short lengths of optical fibre. These are fixed in the focal plane by means of an aperture plate, which has been pre-drilled with holes corresponding to the positions of the target objects. A similar system known as FOCAP (Fibre Optically Coupled Aperture Plate) (Gray et al., 1982) exists at the AAT and another system, OPTOPUS, is in regular use at the Cassegrain focus of the ESO 3.6 m telescope (Lund, 1986). The latter is also permanently linked to a high dispersion spectrograph using a 35 m long fibre link (Avila and D'Odorico, 1988). Wide-angle multi-object spectroscopy has also been achieved by Watson (1984) using the 1.2 m UK Schmidt telescope.

Fibre optic arrays, which reformat an area to one, three or five long slits, have now been manufactured for use with the Manchester echelle spectrometers (Meaburn and Clayton, 1988, in preparation). These devices, conceived by John Meaburn and singularly known as MATADOR (Multi-Aperture Target Area Dissecting Optical Reformatter), have to be physically small in size to fit into the free space within the spectrometer and this requires the fibres to follow curves of relatively high radii of curvature. The bending of a fibre reduces its throughput and enhances an effect which occurs ordinarily in straight fibres (albeit of different reasons) known as focal ratio degradation (FRD), or alternatively decollimation, mode coupling or beam spreading. As the name suggests, this is the angular spreading of the fibre output beam profile when compared with that of the input beam. This effect can result in light loss off the edge of the collimator in the spectrometer, which must be avoided when observing faint sources. It was thus decided that the nature and effects of decollimation and other sources of light loss in both straight and bent fibres should be investigated before building the Matadors for the echelles. In addition, the small size of these devices means that only short lengths of fibre are used and thus the image scrambling properties of such fibres should also be investigated, although for the echelle operating in its primary mode (see Meaburn et al., 1984) ineffective IS is not a problem.

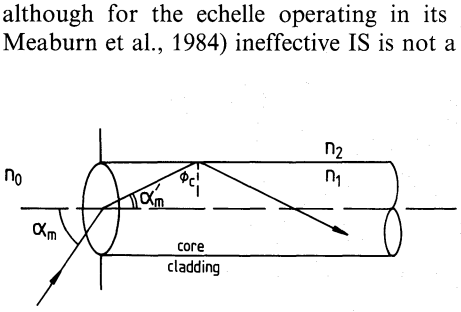

Fig. 1. Schematic diagram of a fibre optic illustrating the concept of numerical aperture

These problems were addressed by first consulting the literature to find what other workers have discovered concerning these phenomena. Various experiments were then undertaken to assess the practicality of small scale fibre optic image reformatters in respect of focal ratio degradation and image scrambling.

2. Focal ratio degradation and image scrambling

2.1. Background information

Optical fibres are basically waveguides for electromagnetic radiation at optical frequencies. Although, in principle, the transmitted radiation always consists of a combination of discrete waveguide modes, distinct patterns can usually only be observed in very small fibres or under special illumination conditions, or both. In astronomical applications, where the fibre is large compared with the wavelength of light, the large number of possible waveguide modes (which increases with the area of the fibre) obscures the individual mode patterns and results in uniform illumination over the output face of the fibre. Under these conditions most of the optical properties of the fibre can be adequately described in terms of geometric optics. For simplicity, the majority of this discussion will deal with fibre optics in these terms.

Consider the case of a straight fibre with a refractive index n_1 embedded in (or clad with) a medium of refractive index n_2 where $n_1 > n_2$. Let a ray of light which passes through the fibre axis (a meridional ray) be incident from a medium of refractive index n_0 onto the perpendicular end face of the fibre at an angle α. This ray will be refracted at the end face and will be totally internally reflected at the fibre wall if its angle of incidence is greater than the critical angle ϕ_c. The maximum value of α for which the ray will be totally reflected can be derived from Snell's law and simple trigonometry with reference to Fig. 1,

$$n_0 \sin\alpha_m = n_1 \sin\alpha'_m = n_1 \cos\phi_c = n_1 (1-\sin^2 \phi_c)^{1/2} . \quad (1)$$

Now $\sin\phi_c = n_2/n_1$ and hence

$$n_0 \sin\alpha_m = n_1 (1-(n_2/n_1)^2)^{1/2} = (n_1^2 - n_2^2)^{1/2} . \quad (2)$$

By analogy with lens optics, the term n_0 is called the *Numerical Aperture* or N.A. of the fibre and is a measure of the light-gathering power. Strictly speaking, the N.A. is defined by the angle at which the cone of light cuts off altogether. Since this is somewhat difficult to determine precisely, the working N.A. is often defined in terms of the angle at which the light input or output falls to 50% of its maximum (axial) value (Kapany, 1967). Most astronomers are happier dealing with focal ratios. These are related to numerical apertures by the approximate relation

$$f \simeq \frac{1}{2\,\text{N.A.}} . \quad (3)$$

Equation (2) applies only to meridional rays in an ideal fibre and hence it is more appropriate to call this the *nominal* numerical aperture. It can be shown (Kapany, 1967) that the nominal N.A. is an underestimation of the light collecting efficiency of a perfect circular fibre, since skew rays (i.e. rays which do not pass through the fibre axis) incident at angles larger than α_m *can* be conducted by perfect circular fibres and it is in fact these rays which dominate the propagation of light down a fibre.

From skew ray calculations, it is possible to define an effective numerical aperture (NAF) which describes the light collecting

capacity of the fibre more accurately. Potter et al. (1963) give a generalised expression for NAF as a function of the indices of refraction. If Fresnel reflections at the faces, losses due to absorption, reflection, and scattering are set to zero, an expression for NAF for this idealised fibre in air is given by

$$(\mathrm{NAF})^2 = 1 - (2/\pi)\,((n_1^2 - n_2^2)\,(1 - n_1^2 + n_2^2))^{1/2} + (1 - 2\,(n_1^2 - n_2^2))\,\cos^{-1}((n_1^2 - n_2^2)^{1/2}))\,. \quad (4)$$

As an example, the effective numerical aperture for the fibres used in the Matador devices ($n_1 = 1.4525$, $n_2 = 1.438$) is

$$\mathrm{NAF} = 1.35 \;\; \mathrm{N.A.} = 0.277 \;\; (f/1.8)\,. \quad (5)$$

In practice, one finds that the limiting angle α_m is not as sharply defined in actual fibres as Eq. (2) implies. Diffraction, striae, and surface irregularities on the fibre wall all tend to decollimate the transmitted light and thereby reduce the effective N.A. This is the focal ratio degradation mentioned in the introduction. Inadequate insulation between fibres can also reduce the N.A., and only an actual measurement of the acceptance angle can produce a true indication of the numerical aperture.

The range of possible values of N.A. for the fibres is limited only by the materials from which they can be drawn. In the case of glass-clad/glass-core fibres this range is considerable. In general, the higher the core glass refractive index, the higher the N.A., but the lower the transmission in the short wavelength end of the spectrum. This is an important consideration when linking spectrographs to telescopes with long lengths of fibre if the extreme violet and UV end of the spectrum is to be studied.

At this point it is important to distinguish between step-index and graded-index fibres. Since the functioning of a fibre as a waveguide depends on total internal reflection, the fibre must be surrounded by a medium of a lower refractive index. Suspending the fibre in air is ineffective since the glass/air interface is easily damaged and thus optical fibres are usually surrounded by some kind of coating of lower index material. This may take the form of a well-defined sheath of cladding, resulting in a step-index fibre, or it may be accomplished by a gradual reduction of the index with distance from the fibre axis, resulting in a graded-index fibre. Graded-index fibres show no degree of focal ratio preservation or image scrambling and will not be discussed further. Throughout this paper, the term fibre refers to step-index fibre.

2.2. *Focal ratio degradation*

Fibres differ optically from perfectly cylindrical waveguides principally by the presence of numerous geometric defects on a scale compared to the fibre core diameter. These *microbends* scatter the axial angles of incidence of guided rays, causing focal ratio degradation. The physical properties, surface structure, inhomogeneities, and variations in diameter thus play an important role in the light conduction properties of a fibre. These vary from fibre to fibre of different materials and manufacturing origin, since they are due mostly to the type of cladding and its method of application during the fibre drawing process. Fibre optics are being made of materials such as glass, quartz, nylon, polystyrene, and other synthetic materials. Investigation has shown, however, that glass or quartz are preferred for optical use, from the standpoint of surface quality, light transmission and homogeneity. Since microbending in fused silica fibres arises mainly from stress on the fibre core induced by cladding and/or jacketting, fibres with cladding materials of low elastic moduli typically show relatively little beam spreading, and viceversa. Heacox (1983) comments that fibres showing sufficiently little beam spreading for practical use also show no detectable increase in beam spreading due to macrobends with radii of approximately 5 cm or greater.

An additional distortion which causes beam spreading is that of *macrobends* which might, for example, occur in transporting the light from a face plate to a spectrograph slit. Finally, beam spreading also arises from *diffraction* at the fibre ends.

Beam spreading in optical fibres not only results in light loss off the spectrograph collimator but if sufficiently severe, can also cause the N.A. of the aperture of the fibre to be exceeded and consequent light loss from the beam will occur. Clearly, it is desirably to keep beam spreading to a minimum. In most fibres beam spreading is a large effect and fibre behaviour in this respect usually dominates selection of a specific fibre for our purposes.

Beam spreading forces the spectrograph designer to chose between the following when incorporating fibre optics into an instrument:

i) Using a collimator designed to accept the original focal ratio, resulting in light loss off the collimator edge. This was necessary in the Manchester echelles since the use of fibre optics with these instruments is only an option.

ii) As i) but re-imaging the output end of the fibres to restore the original focal ratio, resulting in loss of spectrographic resolution. This may be achieved using "microlenses". The use of microlenses to combat the effects of decollimation are discussed later.

iii) Enlarging the spectrograph optics to accept the full output beam without re-imaging. Again, since fibres are only an option, this is not possible with the Manchester echelles. If the fibres were a permanent feature of the spectrometers this could be done, but only at the expense of increasing the diameter of the collimator and grating with no attendant increase in spectral resolution, since the spectrograph input aperture would be correspondingly enlarged. Thus, the design problem would be one of choosing tradeoffs between throughput, resolution and grating diameter.

In the case of the FOCAP system at the AAT, this third option has been adopted. When using FOCAP, the RGO spectrograph has its $f/8$ collimator replaced by an $f/6$ collimator. The faster f-ratio of this collimator increases the projected slit size and thus decreases the effective spectral resolution. However, this is offset by the better throughput resulting from the faster collimator accepting more of the focal ratio degraded beam. The $f/6$ collimator gives 83% transmission efficiency as opposed to 64% with the $f/8$ collimator (Gray et al., 1982).

Heacox (1983) has examined the problem of beam spreading in straight fibres theoretically and concludes that beam spreading losses can be characterised by a single microbending parameter and that these losses are proportional to input focal ratio and the square root of the fibre length. More specifically, by including the effects of diffraction he obtains the following result. For a collimated beam of input angle of incidence θ_0, the distribution of output angles of incidence is approximately given by

$$P(\theta/\theta_0) \propto \exp\left(-\frac{1}{2}\left(\frac{\theta-\theta_0}{\sigma}\right)^2\right), \quad (6)$$

where

$$\sigma = \frac{\lambda}{d_f}\sqrt{\frac{1}{2n^2}\frac{L}{L_D}} + 0.193\,. \quad (7)$$

The numerical constant arises from diffraction. The parameter L_D, characterises the microbend induced beam spreading behaviour of the fibre and can usefully be thought of as the fibre

length for which microbend induced beam spreading is comparable in magnitude to that produced by diffraction.

From this result Heacox derives the all important expression for the fraction of light emergent from a fibre that misses a collimator of focal ratio f, if the input beam is also of focal ratio f (and is uniformly filled) and f is sufficiently small

$$T_{FR} \simeq \sqrt{\frac{8}{\pi}} f\sigma . \tag{8}$$

Clearly, to avoid beam spreading loss we must keep σ small, which requires (among other things) that the fibre length be small in comparison with the value of L_D characterising the fibre. The $L^{1/2}$ dependance of microbend induced beam spreading characterised by Eqs. (7) and (8) is verified by the laboratory test results reported by Gambling et al. (1975).

2.3. *Focal ratio degradation and light loss in bent fibres*

It has been stated that the effective N.A. of a fibre is influenced by diffraction, striae and surface irregularities because they cause decollimation of the light passing through the fibre. An additional cause of this decollimation and also of the reduction of effective N.A. of the fibre is bending. When a fibre is bent, certain rays previously trapped can escape.

The effects of decollimation in bent fibres have been studied theoretically by Potter (1960) who has derived the following expression

$$\Delta \cos \alpha_{out} = \frac{2\, d R \cos \alpha_{in}}{R^2 - (d/2)^2}, \tag{9}$$

where d is the fibre diameter, R is the bend radius, α_{in} is the half-angle of the incident cone, and α_{out} is the half angle of the emergent cone. In the derivation of this formula, however, only meridional rays were considered. In addition, it was assumed that the bending radius is much greater than the fibre radius and that the fibre length is long enough for a large number of reflections to take place along the fibre. For $d \leqq R$ this reduces to

$$\Delta \cos \alpha_{out} = (2\, d/R) \cos \alpha_{in} . \tag{10}$$

Thus, for a parallel beam of light ($\cos \alpha_{in} = 1$) incident on a fibre of 100 μm diameter bent to a radius of 2 cm, $\Delta \alpha_{out} = 8°$. Thus, the decollimation effects of even such a high bending ratio as 200 : 1 can be significant.

The geometric optical properties of fibres and the effects of bending have also been studied by Kapany (1957). He predicted that for an incident cone of light with a half-angle of 40°, meridional rays begins to escape through the walls of an unclad fibre when $R < 3.5\, d$, where R is the bending radius and d is the fibre diameter.

In practice, however, he found that since the rays in the meridional plane contribute little to the total conduction of the bent fibre, the condition for minimum permissible bending is violated because rays in other planes escape from the walls when the cylinder is bent on a radius 20 times its diameter.

Levi (1980) has shown that a ray will escape from a bent fibre if

$$n_2/n_1 < \cos \alpha_m \frac{2R - d}{2R + d} \tag{11}$$

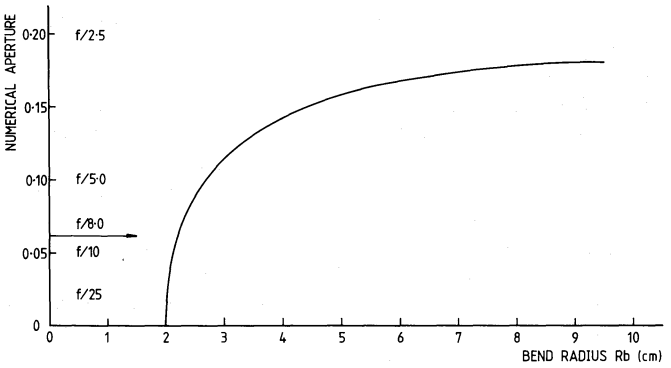

Fig. 2. The variation of numerical aperture of a fibre with bend radius according to Eq. (12)

i.e. the N.A. is reduced by the bending. The cone of rays that are captured by the fibre is now restricted to a smaller semiangle corresponding to a nominal N.A.

$$\text{N.A.} = \left(n_1^2 - n_2^2 \frac{(1+\varrho)^2}{(1-\varrho)^2} \right)^{1/2}, \tag{12}$$

where $\varrho = d/2\, R$. Regarding the meridional ray, therefore, the bending is equivalent to an increase in n_2 by a factor

$$\frac{(1+\varrho)}{(1-\varrho)} \sim 1 + 2\varrho \tag{13}$$

This reduction of N.A. due to bending for a 200 μm fibre, is shown in Fig. 2. This graph shows a cut-off at 2.0 cm In actuality, light may be transported down in the fibre for $R_b < 2$ cm since the analytic description of this curve again only includes meridional rays and in reality it is the skew rays which dominate the propagation of light down an optical fibre.

From Eq. (12) it is clear that for fibres with small index differences, even slight bending can destroy the trapping effectiveness. Since the bend need not extend over a long segment of the fibre, even a slight deviation from straightness, a microbend, can impair trapping significantly and, if such microbends exist in large numbers, they can dominate the attenuation in the fibre.

An alternative way to appreciate why bends in fibres should give rise to losses is to consider the propagation of the light in terms of modes. The part of the mode which is outside of the bend will need to travel faster than that on the inside to maintain a wavefront that is perpendicular to the propagation direction. Now each mode extends, in theory, an infinite distance into the cladding despite the exponential decline of the electric field intensity within it. Consequently, some part of the mode in the cladding will find itself attempting to travel at greater than the velocity of light in that medium and hence the energy associated with this particular part of the mode must be radiated away. It is thus reasonable to deduce that the loss will be greater (a) for bends with smaller radii of curvature, and (b) for those modes which extend most into the cladding. The loss can be generally represented by an absorption coefficient α_B

$$\alpha_B = C \exp\left(\frac{-R_b}{R_c} \right) \tag{14}$$

where C is a constant, R_b, the bending radius and the value of R_c is given by $R_c = d/2\,(\text{N.A.})^2$ (d being the fibre diameter) (Levi, 1980). It is again evident that bends with radii of curvature of order of the magnitude of the fibre radius, microbends, are to be avoided.

It is worth pointing out that the problem of losses due to curvature of optical fibres is far more complex than the simple discussion presented here would indicate. Most of the modern analyses of the problem are carried out in terms of waveguide theory with a view to applications in fibre optic communications. Some of the complications encountered include field deformation caused by bending, which can produce a shift in peak intensity of the output beam, and whispering gallery modes whose curvature losses are independent of fibre radius. Those interested in reading further on these matters should consult Marcuse (1976) and Arnauld (1974) (and references therein) for an introduction to this approach.

Since the use of fibre optic arrays with the Manchester echelle spectrometers is only one of several modes that the instrument may be used in, the spectrometers cannot be remanufactured to accommodate the effects of focal ratio degradation in the fibres. It is necessary to minimize and compensate for FRD in the fibre array itself. Decollimation may be minimized by:

1) Selecting a well manufactured fibre. The amount of FRD induced in a fibre varies from manufacturer to manufacturer for fibres of the same physical dimensions. Tests on the decollimation effects of various commercially available fibres in order to determine their suitability for astronomical applications have been carried out by various workers including Angel et al. (1977), Barden et al. (1981), Heacox (1983) and Powell (1983). Unfortunately, the amount of FRD for a given fibre can vary from batch to batch so it is not possible to define an absolute measure for a given fibre type. In addition, manufacturers are continuously "improving" particular fibres and rationalizing their range of products.

2) Minimizing macrobends in the fibre. Macrobends are unavoidable in the Matador devices. However, careful design has reduced these to a minimum.

3) Minimizing stress in the fibre. Stress induces microbends and fluctuations in the refractive index of the fibre which leads to decollimation. One must avoid pinching of the fibre and care must be taken not to induce stress in the fibres where they join supporting or mounting plates. Stress is one of the major sources of decollimation in fibre optics.

In addition to following the precautions and guidelines listed above to minimize FRD, it is possible to actively compensated for decollimation in the fibre array by the use of microlenses. The term "microlens" is used here to describe several types of optical focussing elements which have dimensions comparable to those of the fibre itself. Discussion of these different types is beyond the scope of this work and the interested reader is referred to Hill et al. (1983) and references therein. These microlenses may be used in two ways:

1) Microlenses may be placed at the output of each fibre to produce the desired focal ratio to match that of the spectrometer. This arrangement has an additional advantage. Any misalignment between the fibre output axis and the spectrometer axis, which would lead to light loss off the edge of the collimator, can be corrected for using the microlenses to align each output beam centrally onto the collimator entrance.

2) An alternative approach pioneered by Hill et al. (1983) is to use a microlens to image the telescope pupil on the fibre core. In this case the microlens acts somewhat like a field lens or Fabry lens. If a similar lens is placed at the output end of the fibre, the pupil imaging optics will convert the effects of FRD in the fibre into an increased image size at the output lens. In the absence of FRD, pupil imaging will preserve seeing disks smaller than the entrance aperture at the expense of perfect image scrambling.

Unfortunately, the use of microlenses with the Matador devices is precluded on the grounds of cost. Instead, care in manufacture has reduced light losses to as low a level as possible and this loss must be accepted.

2.4. Other losses

In addition to the losses already discussed due to the reduction of the N.A. and decollimation, there are two other important sources of losses in transmission which should be discussed at this point, intrinsic line losses and end losses.

2.4.1. Intrinsic line losses

The attenuation of light along a fibre is a complex process involving absorption, scattering, and imperfect reflection. The absorption losses in the visible arise mainly from the presence of impurities. Scattering losses arise from fluctuation in the refractive index through the core material. If the scale of these fluctuations is of the order of $\lambda/10$ or less, then each irregularity acts as a point source scattering centre. This type of scattering is the well-known Rayleigh scattering and is important since it represents the minimum loss that can be obtained in a fibre.

The net effect of the above processes can, fortunately, be expressed for a straight fibre as

$$T = e^{-\alpha L}, \tag{15}$$

where T is the fraction of incident light, L is the length of the fibre and α is defined as the attenuation coefficient. The attenuation coefficient is a function of the input ratio, wavelength and the type of fibre. As the input focal ratio decreases, the number of reflections increase and hence so does the attenuation. Thus, the effective numerical aperture *decreases* with the length of the fibre.

In the case of the Matador devices, the lengths of fibre used are $\sim$6 cm. Figure 1 of Angel et al. (1977) shows the transmission of fused silica fibres as a function of wavelength and fibre length, based on the data of Pinnow et al. (1973). The attenuation from absorption and Rayleigh scattering is included. From this data is was found that a 6 cm length of such fibre would have a transmission of 0.9995 at [O III] 5007 Å and 0.9998 at Hα 6563 Å. Thus, one can conlcude that the effects of attenuation due to the above mentioned processes is totally negligible for the short fibres used in the Matador devices.

2.4.2. End losses

Three main factors contribute to end losses in fibres, the effective numerical aperture of the fibre, Fresnel diffraction from the entrance and exit faces of the fibre and scattering losses resulting from imperfect fibre faces.

The first of these together with the distribution characteristics of the incident light determines the amount of light which can be accepted. The N.A. should be chosen to accept as much of the incident light as possible. This is done by choosing a fibre with the appropriate refractive indices and minimizing macrobends.

The Fresnel reflection coefficient for normal incidence (and practically for all input focal ratios likely to be used in astronomical applications) can be computed from the well-known formula

$$R = ((n_1 - n_0)/(n_1 + n_0))^2 \tag{16}$$

where n_1 is the refractive index of the core glass, n_0 that of the adjacent medium, and R the reflection coefficient for each face.

The combined Fresnel reflection losses for both ends of the fibre is given by

$$R_t = 1 - (1 - R)^2 . \quad (17)$$

For fused silica, $R = 0.035$ but anti-reflection coating could decrease this to, say, 0.02 (Gray, private communication). In these two cases, R_t would be 6.9% and 4.0% respectively. Anti-reflection coating is thus desirable and can most easily be achieved by cementing thin silica plates over the ends of the fibre arrays with silica index matching cement. This would provide a suitable surface for anti-reflection coating, and would also effectively eliminate optical error due to the inaccuracies in end preparation. Scattering losses resulting from imperfect fibre faces might otherwise typically be 3% at each face (Gray, private communication).

Finally, the coupling efficiency, T_c is less than unity due to scattering losses resulting from imperfect fibre faces. Typically, $T_c = 0.97$ for a well polished fibre (Gray, private communication).

2.5. *Image scrambling*

In principal, a meridional ray transmitted by a fibre will remain in the same azimuthal plane throughout its passage, emerging at the same angle α at which it entered. In practice, however, a bundle of rays of small but finite diameter entering at angle α will gradually disperse in azimuth because of the small skew component and the large number of reflections, so as to fill an annulus of a cone of half-angle α upon leaving the fibre. It is this effect which leads to the useful image scrambling property of step-index fibres.

Since step-index optical fibres act as good image scramblers the use of such couplers causes the distribution of light of the collimator to be quite insensitive to the position of the image on the input end of the fibre. This suggests that optical fibre couplers may effectively eliminate errors due to seeing and guiding effects. If this were not the case, incorrect centering of the object could lead to line profile changes or radial velocity errors.

Any structure in the line profile will be within the instrumental profile (which in the case of the Manchester echelle operating in its primary mode is very narrow) and when observing nebula emission lines will be swamped by thermal broadening. For many types of observations, however, involving high dispersion precision spectroscopy of stars, the stability and consistency of illumination of the spectrograph optics are yery important. Tull (1975) and Gray (1976) discuss in particular the problems associated with guiding and scintillation errors in slit spectrographs.

An expression relating the distribution of light on the collimator to the position of the image relative to the centre of the input end of the fibre would be useful. Unfortunately, this is rather a difficult task and as yet no-one has managed to solve it analytically.

However it is possible to make order of magnitude estimates which considering the uncertainties introduced by microbends and macrobends is probably all that a more detailed calculation could hope to achieve.

With an input focal ratio of f (in air), Heacox (1983) has shown that a typical ray will suffer k reflections in traversing a straight fibre where

$$k \simeq \frac{L}{2.9\, dn_1 f} . \quad (18)$$

For the length of fibres used for the Matador devices, this number is of order 10. A typical skew ray follows a broken helical path through the fibre and has its azimuthal co-ordinate (projected onto the fibre face) changed by about k rotations. The fraction of rays suffering a total rotation of *less* than, say, 2π, is about

$$\left(\frac{dn_1 f}{2L}\right)^2 , \quad (19)$$

which for the Matador devices is of order 10^{-3}. With these figures in mind, it may seem dubious that these short fibres are capable of sufficient image scrambling. However, these are only order of magnitude estimates and only actual experimentation will reveal the true degree of image scrambling occurring. In long (~ 10 m) length often used by astronomers to link, for example, a spectrometer to the prime or Cassegrain focus of a telescope, one would expect ~ 500 reflections and only 1 in 10^7 rays to be rotated by less than 2π. In such cases it is easy to see how fibres scramble images so effectively.

2.6. *Image scrambling in bent fibres*

Image scrambling can destroy structure in the radiation pattern produced due to bending of the fibre. However, for *very* short lengths of bent fibre the flux distribution pattern emerging for these fibres illuminated by a point source do show structure. Since the Manchester echelle Matadors are arrays comprised of many short pieces of bent fibre it is important to gain an understanding of light propagation in bent fibres and determine under what circumstances this behaviour becomes relevant to the design of image reformatters. Kapany (1957) conducted various experiments to examine this problem. He found that in general, the change in radiation pattern is observed to be systematic when any of the two variables, (a) the axial length, and (b) the bending radius R/d are varied one at a time. As the axial length is increased, keeping the bending radius constant, the radiation pattern tends to regain symmetry. Similarly, when the bending radius is incrased maintaining the axial length constant, the radiation pattern becomes progressively symmetrical. The difficulties involved in predicting the *precise* shape of radiation patterns are enormous.

3. An experimental investigation of FRD and IS

In this section the results of experiments designed to examine the effects of bending fibres in relation to their focal ratio degrading properties and the degree of image scrambling in both straight and bent short fibres are presented. These were mainly conducted specifically with the design of the Matadors in mind. Many of the experiments are qualitative and were undertaken purely to determine if a particular effect would be important in the Matador devices. In addition, in certain experiments quantitative results were not possible with the equipment used.

Focal ratio degrading measurements on fibres to be used for astronomical instrumentation have been made before (e.g. Barden et al., 1981; Powell, 1983) but only with one dimensional cuts across the output beam. In many of the experiments described here, the entire output beam is mapped in two dimensions by scanning the beam with a pinhole/photomultiplier combination. This is necessary since in the light of the predictions of Eq. (18), it was believed that effective image scrambling may not occur and the output beam will not necessarily be circularly symmetric.

3.1. *Experimental set-up*

A dedicated experimental rig was designed and built to conduct these experiments. Figure 3 illustrates the optical layout of the system.

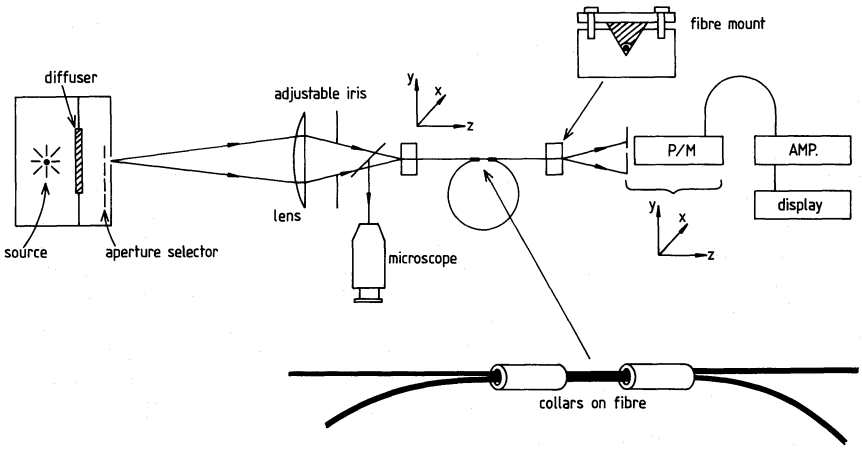

Fig. 3. Schematic diagram of experimental rig

Each component of the apparatus is mounted on a 2.5 m long track of rigid steel. This track has holes along its length and each component has slots in its base through which it is bolted to the track, so that it is possible to achieve any separation between the different components.

The white light source is a 9 V bulb supplied by a stabilised power supply. The light passes through a diffuser and then through an accurately drilled aperture. A self-locking slider system allows any one of four apertures to be used (0.7 mm, 1.0 mm, 1.5 mm, and 2.0 mm in diameter) and accurately centres the selected hole in the optical path. With the component separations used in these experiments, the four aperture diameters correspond to 140 μm, 200 μm, 300 μm, and 400 μm at the input end of the fibre. It is also possible to remove the slider completely and use the surrounding 6.0 mm aperture to ensure complete filling of the fibre input face.

Further along the light path is an adjustable iris. This can be opened and closed to vary the f-ratio of the input beam. For the majority of the experiments undertaken, and unless otherwise stated, this was set to f/8 – the working value of the Manchester echelles. The iris is mounted close to the lens which focuses the beam onto the end of the fibre. This is a 305 mm focal length, f/5.0 Aerostigmatic lens.

The input end of the fibre rests in a slot and is gently (but firmly) held by a small piece of soft wood (see Fig. 3). This was to avoid inducing stress into the fibre. Optical tests were carried out to ensure that no significant stress was caused by this mounting. This mounting is capable of *xyz* motion.

A semi-reflecting sheet of mylar film was placed at 45° between the lens and the fibre end. This can be used to examine the input end of the fibre using a microscope and the *xyz* fibre mounting can be adjusted to centre and focus the image of the illuminated aperture on the end of the fibre.

The far end of the fibre was also mounted in a stress free *xyz* mount, with micrometer heads on the *x* and *y* motions. Attached to this mount is a photomultiplier (p/m) connected to a D.C. amplifier and a luminous digital display. In front of the p/m cathode are a shutter and a 1 mm diameter pinhole. The latter is accurately drilled into a thin (0.8 mm) sheet of aluminium which is placed close to the cathode to minimize projection effects.

The photomultiplier can be moved in the *x* and *y* directions in order to sample different parts of the output beam from the fibre and can be systematically scanned in the *x* and *y* directions in order to sample all parts of the output beam over an area 25 mm by 25 mm. Thus the entire output beam can be mapped without using a 2-dimensional detector, albeit slowly. 1-dimensional scans across a section of the beam are, of course, possible.

Fibre samples are cut to the appropriate length and then ends must be finished to optical flatness. This can be achieved by either of two methods. Firstly, the fibres may be polished by hand using successively finer grades of aluminium oxide lapping film. Alternatively, the fibres may be cleaved with a diamond cutter. This involves gently scoring the fibre and then snapping the end of the fibre off. With practice, this is a fast and effective way to prepare optically flat fibre ends. The samples used in these experiments had their ends prepared using polishing techniques.

Several precautions were taken to prevent spurious effects from influencing the results. Firstly, all the electronics were left on continuously for the duration of the experiments (several months) to ensure that they were operating at maximum stability. Results were found to be repeatable from day to day verifying the stability of the light source and detection system. Secondly, 2-dimensional flat fields were obtained for the pinhole/photomultiplier combination. This was done in order to remove two main effects:

1) At the edges of the detection area, the pinhole in the sheet of finite thickness presents a smaller area to the fibre end and hence the detected intensity is reduced.

2) The finite separation of the pinhole and p/m cathode results in the light which passes through the pinhole falling on different points of the cathode at different positions in the field of detection. Variations in the sensitivity over the area of the p/m cathode can lead to spurious structure in the measured output beam. These variations were measured and their effects were found to be negligible. In any case, many of the results of the experiments are comparative and any spurious beam structure would thus be unimportant.

Finally, it was checked that the mounts holding the ends of the fibres were not inducing stress in the fibres (and hence FRD) by comparing the output beams from a fibre as the mounting clamps were first released and then removed altogether. No variation was found unless the clamps were tightened by an excessive amount.

All experiments were conducted in darkness using a luminous voltmeter which was optically insulated from the rest of the apparatus. Tests undertaken showed light leakage from the imperfect blackout to be undetectable.

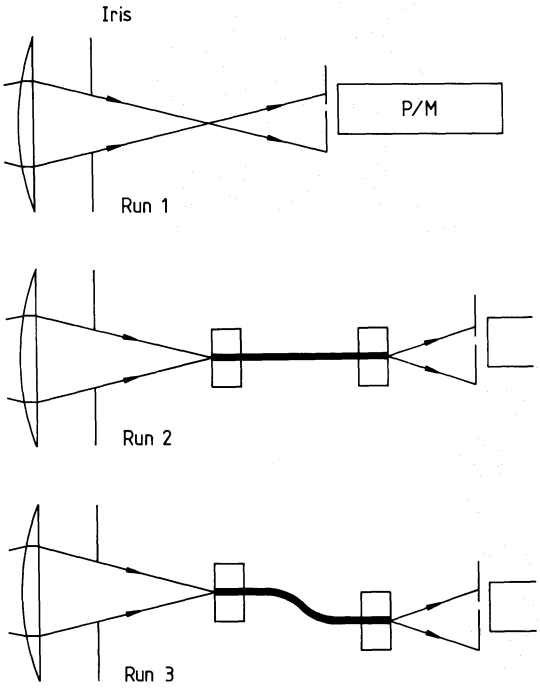

Fig. 4. Details of set up for the first experiment

3.2. The experiments

3.2.1. To compare the relative amounts of FRD due to diffraction, microbends and macrobends

This experiment falls into three parts. Firstly, for run 1 an image of a small illuminated aperture is imaged directly onto the point where the far end of a fibre would normally rest (see Fig. 4). This was done to simulate the output from a straight, idealised fibre, i.e. one in which no focal ratio degradation takes place. This output beam was mapped in 2-dimensions.

For run 2, a 5 cm length of EB 395/425 fibre is introduced into the light path and the optical path is extended by 5 cm. The image of the illuminated aperture now falls onto the near end of the fibre and the far end lies where the image fell in the previous part of the experiment. The output beam is now that from an imperfect but straight fibre. The input beam will suffer FRD due to diffraction and microbends in the fibre. This output beam was mapped.

Finally, for run 3, a macrobend of bend radius $R_b = 1.8$ cm is introduced into the fibre by displacing the far end of the fibre by 1 cm and the output beam was again mapped.

The aperture used was 2.0 mm in diameter which produced a disc of light 400 μm in diameter on the end of the fibre with an input f-ratio of $f/5$. The p/m was scanned in two dimensions to produce 20 by 20 pixel images with a pixel spacing of 1 mm.

The different amounts of FRD occurring in each part of the experiment are best appreciated by examining ratios of the various run images. Figure 5 shows the ratio images run 2/run 1 and run 3/run 2. The FRD caused by just diffraction and imperfections in the fibre can be seen as a ring of excess emission in Fig. 5a. This represents light from the $f/5$ beam in run 1 which has been spread into a faster beam. The output beam from run 3 has been subject to FRD from diffraction, microbends and macrobends. The excess FRD due to the macrobend can be seen in the ratio image 3/2 in Fig. 5b.

We can clearly see that in this case FRD due to the macrobending exceeds that due to diffraction and microbends. This is not unexpected since according to Eq. (8), diffraction effects will lose only 2–3% to a faster than $f/5$ beam. Furthermore, the microbend induced decollimation is proportional to $L^{1/2}$ and in such a short fibre, this is likely to be less than the contribution due to diffraction. Furthermore, the bend was quite drastic, having a minimum radius of curvature of 1.8 cm. Also, the bending will have introduced some degree of stress in the fibre which will induce further microbends and hence FRD. The fraction of light output within $f/5$ in the straight fibre is 78%. For the bend fibre, much light was spread beyond the detection area and so it is not possible to measure the $f/5$ transmission efficiency for this run.

The structure seen in ratio image run 3/run 2 is actual structure in the beam induced by the bending since structure produced by imperfections in the output face of the fibre will be the same in both runs 2 and 3. The structure in the ratio image run 2/run 1 is, however, due to imperfections in the fibre ends. The excess emission to the left of ratio image run 3/run 2 is a consequence of the bend in the fibre which was to the left in the horizontal plane. Clearly, effective image scrambling is not occurring in such a short length of fibre. If it were, the ring would be of even intensity.

3.2.2. To quantitatively compare FRD as a function of macrobend radius in different fibres

In this experiment tests were made of fibres which have already been found to be suitable for astronomical purposes on the grounds of their good focal ratio preserving properties (J.R.Powell, private communication) which were kindly made available by the Royal Greenwich Observatory. These tests were made to measure quantitatively these focal preserving properties of long (1 m) lengths of fibre. Long samples were chosen to ensure effective image scrambling would occur in case any structure was introduced into the radiation pattern in the fibre by the macrobend. The 3 fibres tested were:

Ensign Bickford (EB) 200/230,
Ensign Bickford (EB) 395/425,
Quartz and Silice (QS) 400/600.

100 μm diameter fibres were also available but the detector was insufficiently sensitive to accurately measure the low intensity of light transmitted by these fibres.

The input end of the fibre under test was completely filled with an $f/8$ beam. Since long fibres are being used, the output beam should be circularly symmetric due to image scrambling and thus only 1-dimensional cuts are necessary to accurately determine the degree of beam spreading. In addition, 2-dimensional mapping of the output beams from all three fibres for many different radii of curvature would have taken an inordinate amount of time. Instead, accurate 1-dimensional scans were made with a pixel spacing of 0.5 mm, which represents a small degree of oversampling since the pinhole before the p/m cathode is 1 mm in diameter.

For each fibre it was, however, necessary to do one 2-dimensional scan to accurately locate the centre of the output beam so that a cut directly through the centre of the beam could be made. This scan was also used to verify that the output beam was indeed circularly symmetric when the fibre is bent.

The macrobend was introduced in the middle of the fibre by forming a circular loop of the appropriate radius of curvature. The circular loop was held in the fibre by using two collars as shown in Fig. 3. Great care was taken to ensure that the minimum of stress

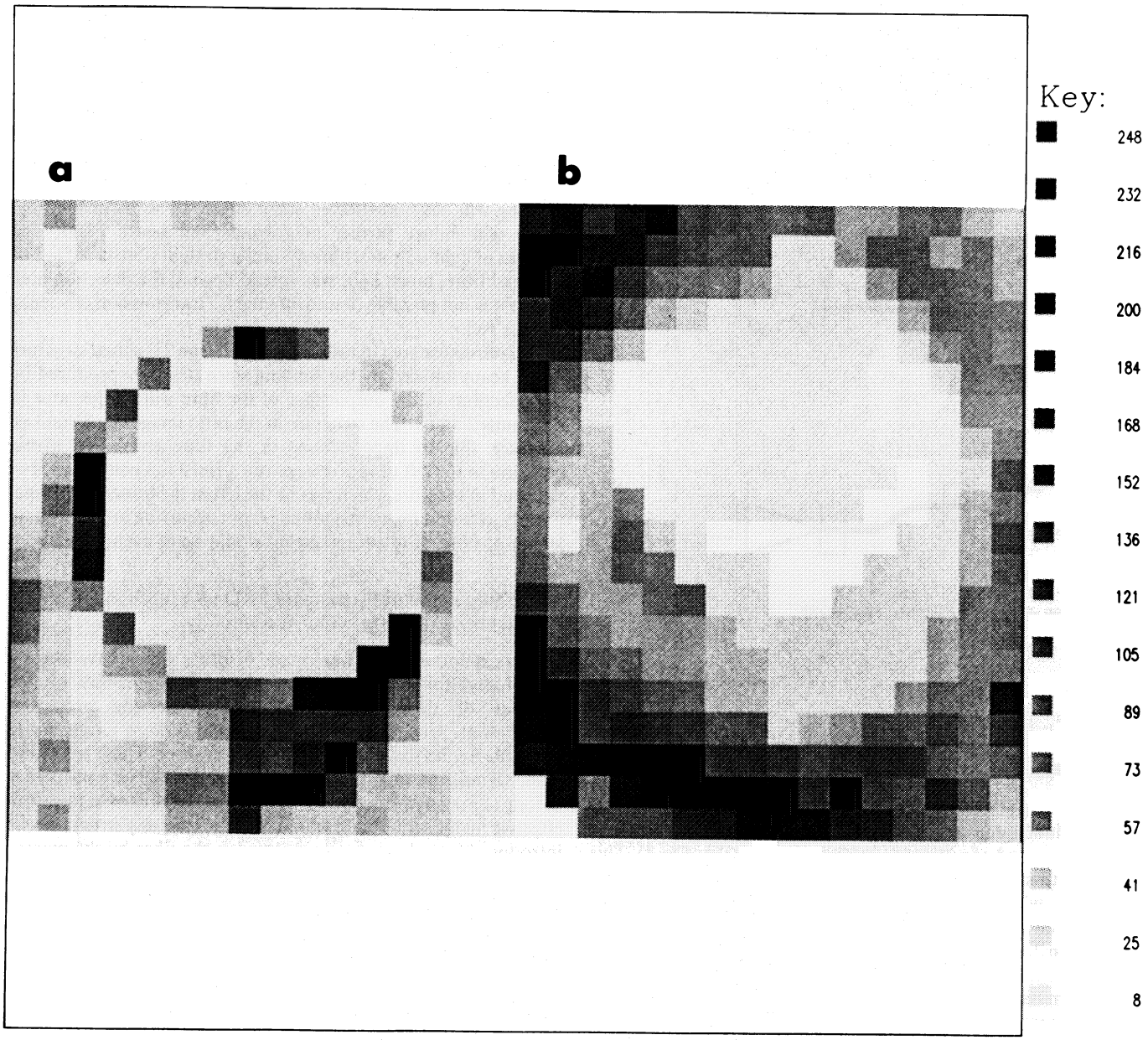

Fig. 5a and b. Ratio images of **a** runs 2 and 1 and **b** runs 3 and 2

was induced in the fibre by these collars. The collars were made wide to distribute the pressure which holds the loop in its shape so as to avoid creating serious microbends. In addition, these collars were made of soft foam so as not to hold the fibre too firmly.

The intensity profiles output from the end of an EB 200/230 fibre for different radii of curvature of the loop are illustrated in Fig. 6. Only 3 profiles are shown for clarity although 11 were actually obtained for this fibre. The effect of macrobend induced FRD is clearly illustrated. The profile anticipated from a straight, perfect fibre (ignoring diffraction effects) is also marked and the reduction of intensity within an $f/8$ beam can be appreciated. In addition, the total intensity under each curve can be seen to be falling with decreasing bend radius as a consequence of the reduction of the N.A. Both of these effects are more clearly illustrated in Figs. 7 and 8 respectively and will be discussed shortly. The irregularity of the profiles is most probably due to imperfections in the fibre face since they show continuity from profile to profile as the bend radius varies and thus are not likely to be due to structure produced in the beam by the bending. Also, such structure would be removed by image scrambling in the long fibre sample used which had a loop to fibre end distance in excess of 50 cm.

Figure 7 shows the total intensity output from the end of the fibre as a function of loop radius. It is quite clear that for radii of curvature (R_b) less than 3 cm, the transmitted intensity begins to decline rapidly and for $R_b = 1$ cm, it has been reduced to 80% of its maximum value.

As mentioned in Sect. 2.3, Kapany (1957) predicted that for meridional rays losses only begin to occur when $R_b < 3.5\,d$ where d is the fibre diameter. However, for skew rays, this condition is

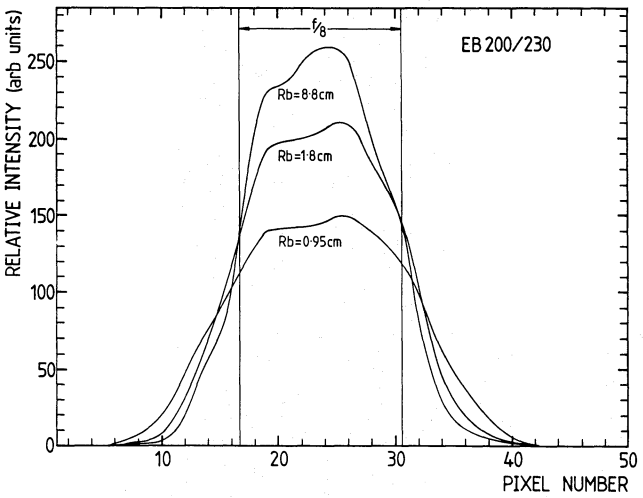

Fig. 6. Three cuts across the output beam for three different radii of curvature of an EB 200/230 fibre

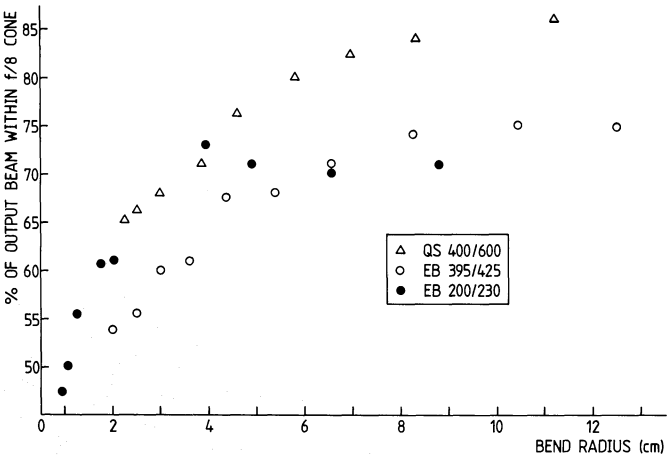

Fig. 8. The percentage of the output beam within an *f*/8 cone as a function of bend radius for three different fibres

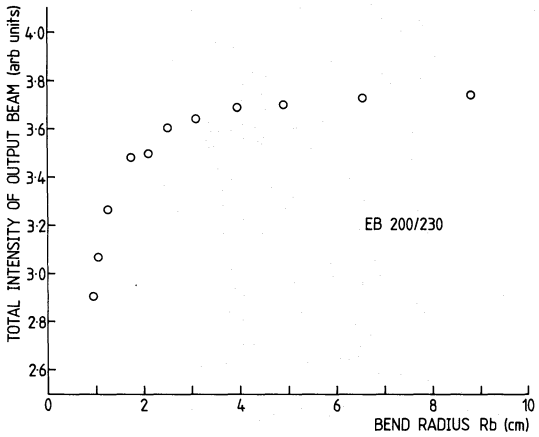

Fig. 7. The variation of output intensity as a function of bend radius for an EB 200/230 fibre

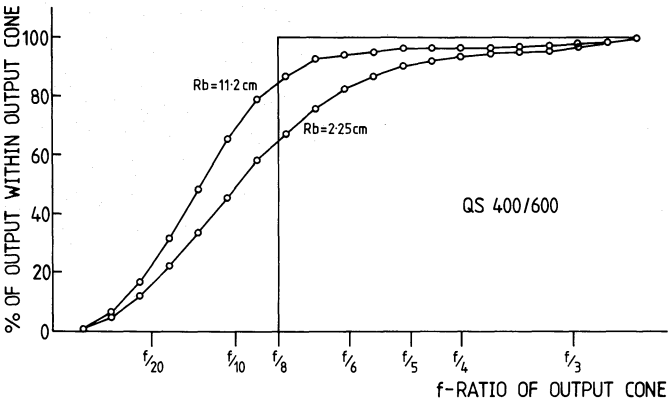

Fig. 9. The percentage of output light within a given output cone as a function of *f*-ratio of the output cone for two bend radii for a QS 400/600 fibre

violated because these rays strike the bent fibre wall at an angle less than the critical incidence and therefore escape. He found that light starts escaping to a serious degree when R_b/d approaches 20. For the EB 200/230 fibre, this occurs when $R_b/d < 50$.

This effect is a consequence of geometric optics and will occur even in a perfectly manufactured fibre. However, in this particular experiment the FRD produced by both microbends and the macrobend will, of course, also lead to some loss of light through the fibre wall.

The shape of this curve cannot be predicted analytically save for meridional rays which play only a minor part on the conduction of light down fibre optics. The effects of both the meridional and skew components might, however, be simulated using ray tracing programmes and the transmission at different R_b/d ratios for a perfect fibre could then be predicted. In a more sophisticated version the effects of imperfections in the core/cladding interface might be taken into effect if suitable parameters could be found.

Figure 8 shows the variation of the fraction of the total intensity output from the fibre that falls within an *f*/8 beam as a function of bend radius for the three different fibres.

The graphs for all three fibres clearly show a reduction in the amount of light in a beam slower than *f*/8 as the radius of curvature decreases. This reduction is in addition to that shown in Fig. 7 due to loss through the sides of the fibre since the values shown in Fig. 8 are fractions of the total *output* of the fibre. This was done to illustrate what fraction of the light is being lost due to FRD as opposed to the reduction in N.A. of the fibre due to bending.

From this graph we can see that typically at a radius of curvature of 3 cm, the fraction of light transmitted within *f*/8 is down to 75–80% compared with the intensity for large values of radii of curvature. The fraction of light lost at high radii of curvature where the curves are nearly horizontal, must be due to FRD due to microbends in the relatively long 1 m fibres and diffraction effects.

The variation in vertical displacement of the flat sections of the curves thus represents a variation in the beam spreading properties of each particular fibre type. All fibres were the same length and so there is no dependance of FRD on length to allow for. The QS fibre would appear to be significantly superior to the EB fibres, having a 15% greater *f*/8 throughput at large radii of curvature.

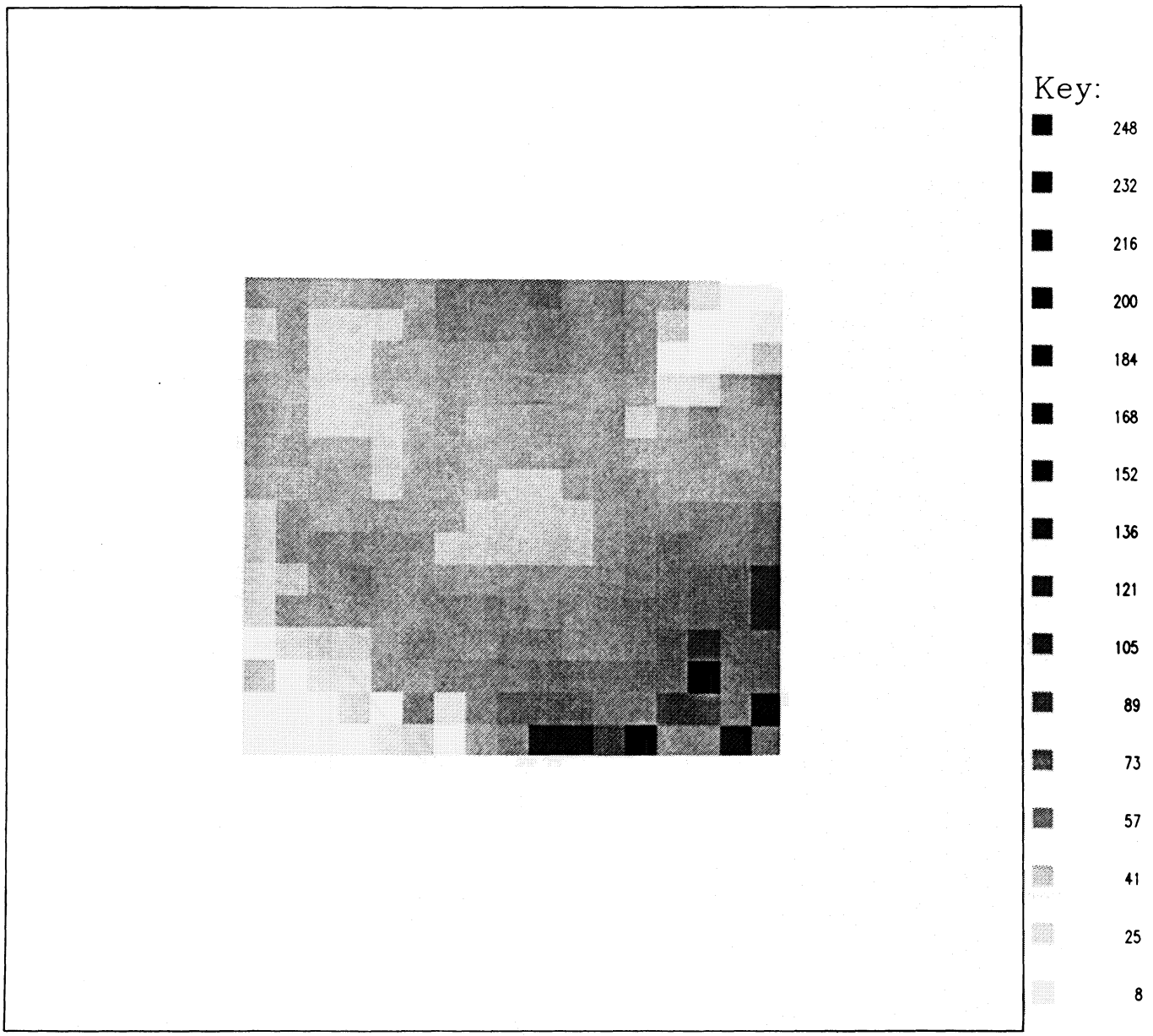

Fig. 10. Ratio image of the output beams from a straight and a severely bent short fibre

The horizontal displacement and compression of the 200 μm core diameter fibre core is merely due to the fact that it is the ratio R_b/d which determines the FRD due to bending (Potter, 1960). If all the points were plotted against a scale of R_b/d, they would all show approximately the same shape.

It should be pointed out that the attempt to deconvolve the effect of FRD due to bending and the reduction in N.A. due to bending by normalizing the curves of the fraction of light with an $f/8$ beam to the total output intensity from the fibre can only be partially successful. This is because the effects of FRD in the fibre will also cause loss of light through the sides of the fibre as well as the geometric effects of bending which will cause losses in both real and perfect fibres. Hence, the numerical values of the FRD to faster than $f/8$, obtainable from Fig. 8, for a given fibre at a given bend radius are not absolute but should give some indication of relative performance.

An alternatively way to interpret these results, which allows one to determine what fraction of light is within any given f-ratio in the output beam, is illustrated in Fig. 9. For clarity, only two values of radius of curvature are shown for the QS 400/600 fibre. The graph is a plot of % of transmitted light within a beam of a given f-ratio against f-ratio. The abscissa is non-linear in f-ratio but is linear in beam radius at the detector. Ideally, one would like the curve for the straight fibre but this would involve dismounting one end of the fibre to remove the collars forming the loop and it is not possible with the current apparatus to guarantee replacing the end in exactly the same place. Hence, the values for the largest radius of curvature used instead. From Fig. 8 it can be seen that the QS 400/600 fibre curve at $R_b = 11.2$, the % of light within an $f/8$ beam is close to its maximum value, i.e. that which it would have in a striaght fibre. Hence, using the values in Fig. 9 for $R_b = 11.2$ is a good approximation to $R_b = \infty$. With this sort of

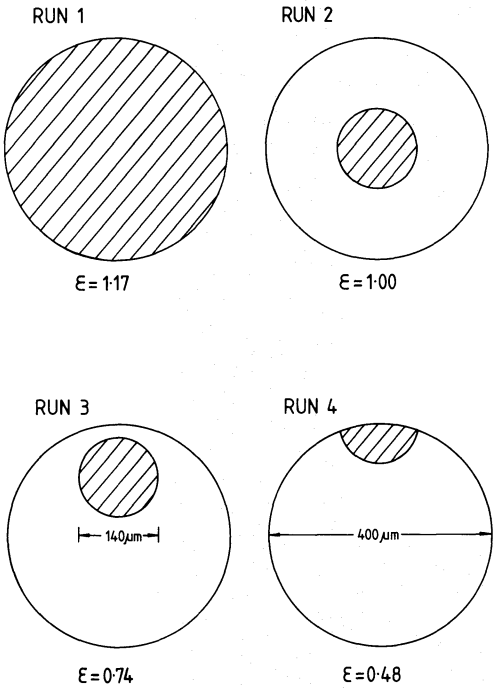

Fig. 11. The size and position of the aperture image at the input end of the fibre in experiment 5

representation, the fraction of light within any output f-ratio, for a given bend radius and fibre, can be read directly off the graph. For example, for the QS 400/600 fibre 85% is within $f/8$ for $R_b = 11.2$ cm but only 65% for $R_b = 2.25$ cm.

This type of graph can be used to judge what improvement in throughput can be achieved by, say, using a faster collimator or increasing the bend radius of the fibres.

3.2.3. To examine the effects of localised stress on FRD

Localised stress on a fibre can produce a microbend of low radius of curvature. As shown in Sect. 2.3, this will lead to a serious amount of FRD. This can be illustrated by placing the detector pinhole at the centre of the output beam of a fibre and pinching the fibre between ones fingers. The intensity at the centre of the beam is reduced by a factor of 2 as the beam is spread into a wider cone. If the fibre is pinched between two finger nails, the reduction in intensity is a factor of 5. If the same fibre is bent in various different ways the decrease in the intensity of the maximum falls by only 20%.

The effects of localised stress can most dramatically and easily be shown in real time using a laser. A beam injected into the end of a perfect fibre at an angle θ will emerge from the other end as a hollow cone of light of semi-angle θ due to the image scrambling properties of step-index fibres. This will appear as a thin annulus when projected onto a screen. However, in a real fibre, FRD takes place and the width of the ring is broadened. This system can be used to qualitatively the beam spreading due to stress induced microbends and that due to macrobends.

A 1 m length of EB 200/230 fibre was illuminated at an angle of 30° by the laser beam and a thin annulus was observed on the screen placed beyond the far end of the fibre. The fibre was pinched between finger nails and the width of the annulus increases approximately 10 fold. However, when a loop was introduced into the fibre, no visible widening of the annulus could be detected until a bending radius of only 1 cm was reached. This is far less than any bending radius likely to be used in any actual instrument.

Quite clearly the presence of a low radii of curvature microbend completely dominates the beam spreading properties of a fibre. Such microbends are most likely to be induced in the fibre at their ends where they connect to other components of an instrument. Great care must be taken to ensure that the very minimum of stress is produced at these points.

3.2.4. To examine the effects of severe macrobending on a short fibre

This experiment was conducted to see if the drastic bending of a short fibre would induce any structure into the beam within the fibre which could not be sufficiently image scrambled before leaving the fibre.

A 6 cm length of EB 200/230 was used since the dimensions of this fibre closely match those which were to be used in the first Matadors. The radiation pattern from the fibre was measured both when straight and when a macrobend of a small radius (<2 cm) had been placed in the fibre. This was done so that the output from the straight fibre could be used as a control to remove any structure in the output beam of the bent fibre which was due to defects in the finishing of the end of the fibre.

Figure 10 shows the ratio of the images of the two output beams. Only a marginal amount of structure has been introduced into the radiation pattern of the output beam by the macrobend. This can be seen as the white (dark) patches at the bottom left and top right of Fig. 10 which are in line with the plane of the bend in the fibre. As expected, some degree of FRD is also shown as a reduction of intensity at the centre. Full image scrambling is not taking place in these short fibres, as was anticipated by Eq. (18).

In addition, the total intensity of the output beam in the straight fibre is 60% greater than that in the bent fibre beam. This is a consequence of the reduction of the N.A. due to the bending and light being spread by FRD beyond the edge of the field of detection.

3.2.5. To examine the image scrambling properties of short fibres

In this final experiment the image scrambling (IS) properties of short bent fibres are examined as the input beam is varied in size and position. This was done to attempt to simulate a star wandering over the input end of a fibre due to seeing and telescope tracking effects in order to see if the image scrambling properties of short fibres are sufficient to avoid zonal errors. The estimations of the IS properties of short fibres (Heacox, 1983, 1986) presented in Sect. 2.5 imply that the number of reflections occurring in the fibre is small and may not provide effective image scrambling. However, Heacox's treatment is at an elementary level and the only sure way to determine the actual effects is to simulate the situation in the laboratory.

In the case of the Manchester echelle fibres, this is not a critical problem since it is used on extended sources and each fibre will be evenly illuminated when seeing effects are taken into account. In addition, any modification to the line profiles will occur within the narrow instrumental profile and such modifications will generally be swamped by thermal broadening. However, it is an important property of fibres which should be investigated.

A straight 5 cm length of QS 400/600 fibre was mounted in the apparatus and then the output end mount was displaced sideways 1 cm to produce a kink in the fibre akin to that in the Matador devices, albeit with a far smaller minimum radius of curvature. A 1200 μm diameter $f/5$ beam was shone onto the end of the fibre and completely filled it. The output beam was mapped in 2-dimensions

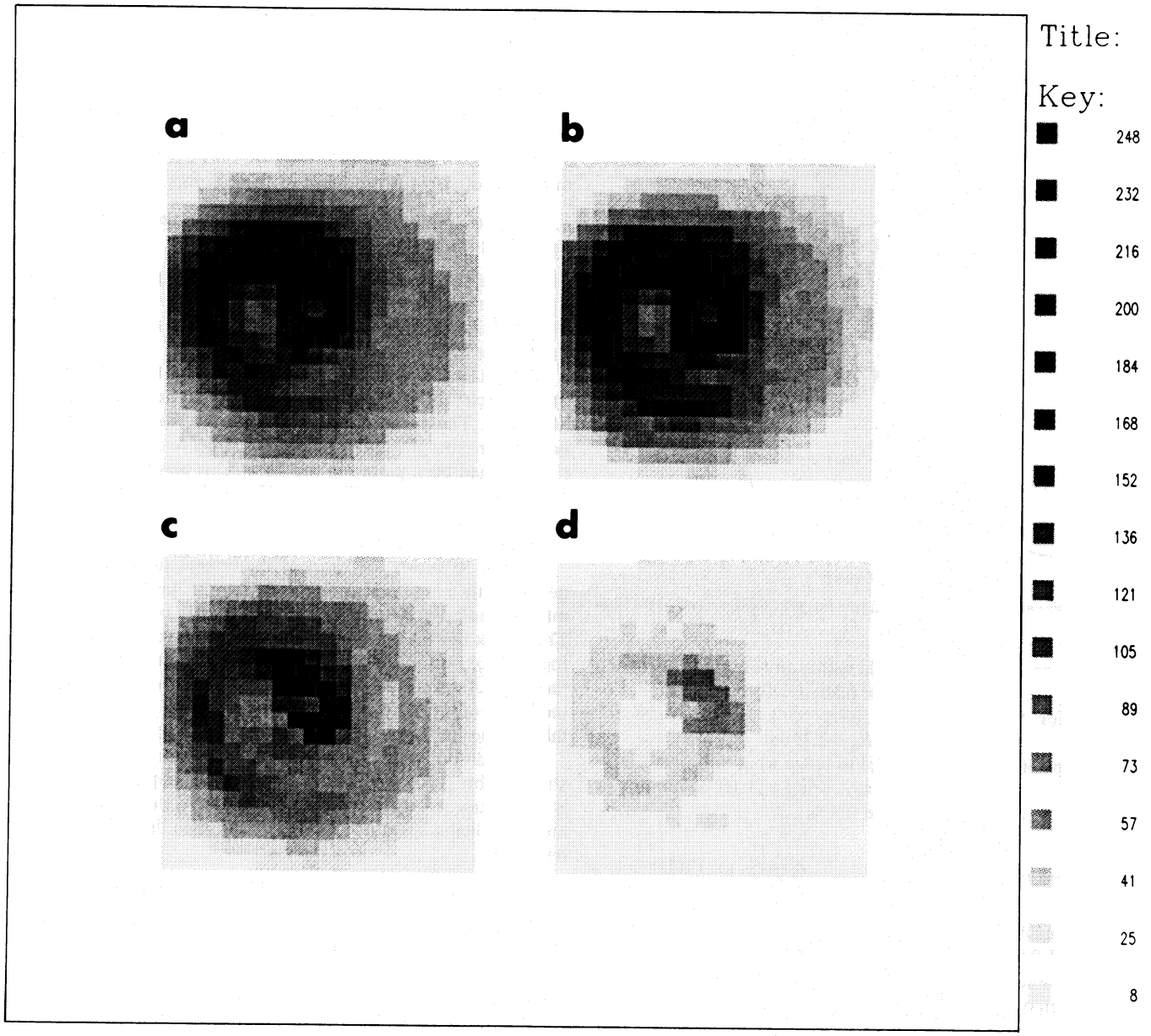

Fig. 12a–d. Greyscales of the output beams from the four runs described in Sect. 3.2.5 and illustrated in Fig. 11

to produce a 20 by 20 pixel image. A 140 μm diameter beam was then input into the very centre of the fibre. This was accurately positioned using the microscope system described in Sect. 3.1. Again the output beam was mapped. The beam was then offset from the centre of the fibre by first 100 μm and then 200 μm (see Fig. 11) and the output beams for these arrangements were also mapped.

Greyscale images of the four output beams mapped are shown in Fig. 12. Below the diagram for each run in Fig. 11 is the total relative intensity of the output beam for that run. These have been corrected to allow for the size of the input beam on the core of the fibre and thus gives some indication of the relative efficiency of the fibre under different conditions of illumination. For example, in run 4 part of the beam is not incident on the fibre core and the total output intensity has been suitably weighted. It can be seen that from runs 2, 3 and 4 that displacing the input beam does affect the throughput efficiency of the fibre when the beam is displaced from the centre of the fibre face. The high throughput of run 1 is believed to be due to the oversized beam illuminating the cladding of the fibre and light leaking from the cladding into the core. Propagation of light in the cladding can usually be ignored since it will soon be attenuated as it strikes the interface of the cladding and protective jacket.

The greyscale representations of the output beams show no variation in structure as the input beam moves over the end of the fibre. The structure seen is due to imperfect IS due to the bend in the fibre and imperfections in the fibre and surfaces.

As the beam is displaced from the centre of the fibre, the greyscale images also suggest that there is a slight concentration of light towards the centre of the beam. The ratio images of run 3/run 2 and run 4/run 2 (not shown here) confirm this. However, the effect is negligible and the variation of the fraction of the total output intensity of the beam within any given *f*-ratio for runs 2, 3, and 4 is at most 3%.

It would thus appear that for the short, bent fibre sample used, the position of the input beam on the fibre input end does not significantly affect the structure of the output beam or produce excess FRD although there is a reduction in the total transmission efficiency down the fibre.

4. Conclusions

One of the obvious areas of interest which was not investigated was that of the variation of FRD variation of FRD with input *f*-ratio. This was because this topic has already been studied experimentally by various other workers and their findings are available in the literature. For example, Barden et al. (1981) and Powell (1983) have studied how well different input focal ratios are preserved during transmission down a long fibre. Most of the experiments described here were carried out with an input focal ratio of *f*/8 to simulate the beam that would be incident on a fibre used with the Manchester echelles.

They found that generally smaller fibres yield better performance with respect to focal ratio preservation, despite diffraction effects, but more importantly that minimum losses through FRD can be achieved by keeping the beam at its highest acceptable ratio within the fibre.

The results of these experiments were mostly obtained with the apparatus working at the limits of its ability. To investigate the fibre properties studied here in greater detail and in a more systematic way would require redesigning the equipment. The most dramatic improvement would be to use an integrating TV camera as the detector. This would provide a real time (or near real time) true 2-dimensional detector. This would provide a huge saving in time since the complete beam could be mapped at far higher resolution in seconds as opposed to the scanning method used in these experiments which took up to 4 hours for a full 25 by 25 pixel mapping.

Secondly, it would be possible to immediately see the effects of, say, bending or stressing the fibre on the output beam and thus a far more comprehensive study than that presented here could be undertaken.

In addition, since these experiments were conducted, an automatic polishing machine has been acquired and fibres with near perfectly finished ends could now be used and structure and additional FRD in the output beam due to deficiencies in polishing the ends would be removed.

In conclusion, it has been found that:

1) Image scrambling is incomplete in short fibres [as predicted by Eq. (18)] but will not affect observations made with the Manchester echelles in the primary mode. Velocity determinations while in the secondary low dispersion mode may be subject to error.

2) The effects of macrobends on various different fibres have been quantitatively measured. Bends of large radii of curvature are found not to produce a significant amount of excess FRD over that naturally occurring in the fibres. Thus, large radius macrobends may be tolerated in the Matadors.

3) Localised stress dominates FRD in a fibre and must be avoided both in manufacture and use at all cost.

4) The position of a source on the end of the fibre determines the transmission efficiency of a fibre.

Acknowledgements. The author would like to thank a number of people in connection with the work presented in this paper. The first of these is my research supervisor John Meaburn who suggested the Matador device concept and that I should conduct an experimental investigation into the transmission properties of fibres.

In addition, I would like to thank Don Gregory who built the experimental rig with such precision and Dick Carling for his work with the Matadors themselves; Ralph Powell and Cyril Taylor of the RGO for their advice and for supplying the fibres used in the tests and John Rowcroft for producing the line diagrams.

The author would also like to acknowledge the S.E.R.C. for the research grants awarded to John Meaburn which financed this work.

References

Angel, J.R.P., Adams, M.T., Boroson, T.A., Moore, R.L.: 1977, *Astrophys. J.* **218**, 776
Arnauld, J.: 1974, *Bell System Tech. J.* **53**, 1979
Avila, G., D'Odorico, S.: 1988, *Proceedings of the ESO VLT Symposium*, Garching, March 1988., ed. M.H. Ulrich (in press)
Barden, S.C., Ramsey, L.W., Truax, R.J.: 1981, *Publ. Astron. Soc. Pacific* **93**, 154
Gambling, W.A., Payne, D.N., Matsumura, H.: 1975, *Appl. Optics* **14**, 1538
Gray, D.F.: 1976, *The Observation and Analysis of Stellar Photospheres*, Wiley, New York
Gray, P.M., Phillips, M.M., Turtle, A.J., Ellis, R.: 1982, *Proc. Am. Soc. Astron.* **4**, 447
Heacox, W.D.: 1983, informal preprint
Heacox, W.D.: 1986, *Astron. J.* **92**, 219
Heel, A.C.S. van: 1954, *Nature* **173**, 39
Hill, J.M., Angel, J.R.P., Richardson, E.H.: 1983, *Proc. S.P.I.E.* **445**, 85
Hill, J.M., Angel, J.R.P., Scott, J.S., Lindley, D., Hintzen, P.: 1980, *Astrophys. J.* **242**, L 69
Hill, J.M., Angel, J.R.P., Scott, J.S., Lindley, D., Hintzen, P.: 1982, *Proc. S.P.I.E.* **331**, 279
Kapany, N.S.: 1955, Proc. Symp. *Astronomical optics and related subjects*, Manchester University
Kapany, N.S.: 1957, *J. Opt. Soc. America* **47**, 413
Kapany, N.S.: 1967, *Fibre Optics, Principles and Applications*, Academic Press, New York
Levi, L.: 1980, *Applied Optics, a Guide to Optical System Design*, Vol. 2, Wiley, New York
Lund, G.: 1984, *IAU Coll.* No. 79, p. 617, eds. M.H. Ulrich, K. Kjar
Lund, G.: 1986, *ESO Operating Manual* No. 6
Marcuse, D.: 1976, *J. Opt. Soc. America* **66**, 216
Meaburn, J., Blundell, B., Carling, R., Gregory, D.E., Keir, D.F., Wynne, C.G.: 1984, *Monthly Notices Roy. Astron. Soc.* **210**, 463
Pinnow, D.A., Rich, T.C., Ostermayer, F.W., Dimineco, M.: 1973, *Appl. Phys. Letters* **22**, 527
Potter, R.J.: 1960, Ph.D. Thesis, University of Rochester, New York
Potter, R.J., Donath, E., Tynan, R.: 1963, *J. Opt. Soc. America* **53**, 256
Powell, J.R., 1983, *Proc. S.P.I.E.* **445**, 77
Taylor, K., Atherton, P.D.: 1980, *Monthly Notices Roy. Astron. Soc.* **191**, 675
Tull, R.G.: 1975, ESO/CERN conference *Instrumentation for Large Telescopes*
Tyndall, J.: 1854, *Proc. R. Inst.* **1**, 446
Watson, F.G.: 1984, *Monthly Notices Roy. Astron. Soc.* **206**, 661